



Article Info

Received: 20th April 2024

Revised: 10th June 2024

Accepted: 14th June 2024

¹Department of Physics, Sokoto State University, Sokoto Nigeria

²Department of Mathematics, Sokoto State University, Sokoto Nigeria

*Corresponding author's email:

usman.iliyasu@ssu.edu.ng

ORCID identifier (0000-0001-6476-3654)

Cite this: *CaJoST*, 2024, 2, 121-130

Effect of MnO₂ on the optical, elastic, mechanical, and radiation shielding performance of bismuth silicate glass

Usman Iliyasu¹, Anas Shehu¹, and Ahmad Rufa'i²

The effect of MnO₂ on the optical, elastic, mechanical, and radiation shielding performance of xMnO₂+(60-x)Bi₂O₃+40SiO₂ glass system have been studied. The refractive index improved by 38% as 20 mol% of MnO₂ is doped into the bismuth silicate glass. The elastic and mechanical properties were estimated using the Makishima-Mackenzie's model. The young modulus improved from 298.61 to 331.28 Gpa and the microhardness increased by 9.25% as 20 mol% of MnO₂ doped into the glass structure. The radiation attenuation properties were investigated using the Phy-X/PSD and XCOM in the photon energy range 0.015-15 MeV. The encoded 0MnBiSi glass sample has lowest half value layer, and mean free path. The findings show that replacing part of Bi₂O₃ with MnO₂ improves optical, elastic, and mechanical properties while decreasing attenuation quality. All the glasses investigated, give better attenuation properties than certain glass proposed for radiation shielding.

Keywords: Silicate glasses; Bismuth oxide; Linear attenuation coefficient; Mass attenuation coefficient; Phy-X/PSD; XCOM.

1. Introduction

Humans are exposed not only to natural radiation, but also to radiation from various anthropogenic sources. Gamma rays and X-rays emitted for use in radiotherapy applications are the most common type. ⁹⁹Tc, ¹²³I, ¹³¹I, ⁶⁷Ga, ⁶⁰Co are examples of commonly used radioactive tracers to evaluate a specific organ of the human body. However, if ionizing radiation is not utilized appropriately, it can endanger personnel, equipment, and the environment [1].

Many researchers have been seeking for appropriate glass compositions that have excellent physical, elastic, mechanical, thermal, and shielding properties. Silicate glass doped heavy metal and transition metal have been suggested for radiation attenuation.

Silicates (SiO₂) belong to a group of oxide glass formers that can covalently bond with heavy and transition metal oxides to form excellent and transparent glass within the visible light [2]. Vishwanath et al. [3] investigated and compared the radiation shielding properties of silicate and borate glasses containing heavy metal oxide. The bismuth silicate glass was found to have a greater Z_{eff} and thus a higher gamma absorption cross section than the other glasses. Tekin et al. [4] investigated the gamma and neutron shielding properties of sodium-calcium-phosphate and silicate bioactive glasses, According to the

findings, silicate glass appears to be a better material for radiation shielding from both photons and neutrons..

Bismuth oxide (Bi₂O₃), a heavy metal oxide with a high density of 8.9 g/cm³, exhibits glass-forming and modifying properties due to its BiO₆ and BiO₃ pyramidal units. When added to a glass system, enhances glass density and increases photon absorption [5]. Previous work by Halima et al. [6] and Boukhris et al. suggested that inclusion of Bi₂O₃ into glass matrix improved the physical and radiation shielding ability.

Transition metals (Fe, Co, Cr, Cu, Ni, and Zn) are commonly used as dopants at low levels to modify the physical and mechanical properties of glass. These metals have been shown to enhance ionic strength, improve optical transparency and strengthen mechanical properties [7-9]. The inclusion of MgO is expected to improve the examined glass's elastic and mechanical properties. Mechanical strength of glasses is critical in radiation shielding because it influences their ability to resist radiation while retaining structural integrity.

The study investigates the effect of manganese oxide on bismuth silicate glass, focusing on its elastic, mechanical, and radiation shielding properties. The research uses the Makishima-

Mackenzie model and Phy-X/PSD to analyze and simulate the properties, aiming to understand how manganese oxide influence the overall performance of the glass.

2. Materials and Methods

The bismuth silicate doped manganese glass in the form of $(60-x)\text{Bi}_2\text{O}_3 + \text{SiO}_2 + x \text{MnO}_2$ where $x = 0, 5, 10, 15,$ and 20 is selected for this work. The glass system was manufactured using melt

Table 1. Chemical composition and density of the fabricated glass

Sample code	Bi_2O_3 (mol%)	SiO_2 (mol%)	MnO_2 (mol%)	Mn (w.t%)	O (w.t%)	Bi (w.t%)	Si (w.t%)	Density g/cm ³	Molar volume cm ³ /mol
0MnBisi	60	40	0	0	0.137	0.826	0.037	6.796	44.71
5MnBisi	55	40	5	0.0096	0.1433	0.8076	0.0395	6.412	44.4
10MnBisi	50	40	10	0.0207	0.1505	0.7865	0.0423	6.198	42.87
15MnBisi	45	40	15	0.0334	0.1589	0.7622	0.0455	6.162	40.05
20MnBisi	40	40	20	0.0482	0.1686	0.7339	0.0493	6.142	37.09

2.1 Optical study

The refractive index is an optical property that describes the transparency of a glass and is influenced by its composition. Changes in refractive index directly affect other optical parameters such as, dielectric constant, electric susceptibility, molar refractivity. The refractive index (n) is determined using the relation [11]:

$$\frac{n^2-1}{n^2+2} = 1 - \sqrt{E_{opt}/20} \quad (1)$$

where E_{opt} represent the optical band gap energy.

Molar refractive index (R_m) is a parameter that is directly affected by the refractive index of glass and is calculated using the equation [12]:

$$R_m = (n^2 - 1)/(n^2 + 2) \quad (2)$$

The electric susceptibility (χ) of the investigated MnBiSi glasses is strongly connected to the dielectric constant (ϵ) and is determined using the following relation [13]:

$$\chi = (\epsilon - 1)/4\pi \quad (3)$$

The optical (η) measures an ion's ability to attract electrons from neighbouring oxide ions, forming stronger bonds. The higher the ion's electronegativity, the tighter the bonds between the network ions, indicating a stronger attraction to the bonded oxide ions. [14].

$$\eta = 0.2668E_b \quad (4)$$

quench procedures at temperatures ranging from 1100 to 1150° C, depending on the composition, and then annealed at 350° C in a muffle furnace for 3 hours before being gradually cooled to room temperature. The glass densities, molar volume, and optical band gap energy can be found in Dult *et al.* [10]. The sample glasses are coded 0MnBiSi, 5MnBiSi, 10MnBiSi, 15MnBiSi, 20MnBiSi for identification. Table 1 shows the compositional ratio of the composite.

Other optical parameters that depend on electronegativity are electron polarizability (α^e) and optical basicity (Λ) [14]:

$$\alpha^e = -0.9\eta + 3.5 \quad (5)$$

$$\Lambda = -0.5\eta + 1.7 \quad (6)$$

The transmission coefficient T_c and reflection loss was determined to estimate the fraction of light that the investigated glass can transmit or loss in the visible region using the following relations [12]:

$$T_c = 2n/n^2 + 1 \quad (7)$$

While the reflection loss at the surface due to scattering;

$$R_l = (n - 1/n + 1)^2 \quad (8)$$

Metallization criteria $M(n)$ is a parameter used in assessing the insulating behavior and estimates the extend a glass becomes metallic given by the relation [15]:

$$M = (R_m/V_m) - 1 \quad (9)$$

For non-metallic material. the permissible value of $M(n)$ lies in the range between $(0 < R_m/V_m < 1)$ [15].

2.2 Elastic and mechanical properties

The elastic and mechanical properties of shielding glasses are crucial in determining their ability to withstand radiation damage and maintain their structural integrity over time.

These properties, predicted using Makishima-Mackenzie's models, play a key role in evaluating the effectiveness of glasses developed for radiation shielding applications [16]. The model is estimated from the molar volume (V_m), density (ρ), atomic packing factor (V_i), and dissociation energy (Q_i) of the glass. The total dissociation energy of the glass composition can be computed using the following equations [17]:

$$Q_t = \sum_i Q_j w_j \quad (10)$$

where $\sum_j Q_j w_j$ represent sum of the dissociation energy and molar weight fraction w_j of the j th component over all glass mixture components.

The formula relating the Young Modulus (E_t) to the total packing density and total dissociation energy (G_t) is expressed as [17]:

$$E_t = 8.36 V_t G_t \quad (11)$$

where V_t denotes the total atomic packing density and can be expressed via relation [17]:

$$V_t = \frac{\rho}{M} \sum_i w_j V_j \quad (12)$$

where V_j denotes the packing factor and is calculated using the relation for a metal oxide of the form $A_X O_Y$ [17]:

$$V_j = N_A \frac{4}{3\pi} (Y R_A^3 + Z R_O^3) \quad (13)$$

where R_A and R_O is the ionic radii for the metal and oxygen.

The bulk modulus K_t , shear modulus S_t , and longitudinal L_t can be expressed by the following relations [18]:

$$K_t = 10 V_t^2 Q_t \quad (14)$$

$$S_t = \frac{3K_t}{10.2V_t - 1} \quad (15)$$

$$L_t = K_t + \frac{4S_t}{3} \quad (16)$$

The mechanical parameters including the Poisson's ration P_r , micro-hardness H , and fractional bond connectivity F_r , are calculated by the following equations [18]:

$$P_r = 0.5 - \frac{1}{7V_t} \quad (17)$$

$$H_m = \frac{(1-2P_r)E_t}{6(1+P)} \quad (18)$$

$$F_r = 4 \frac{S_t}{K_t} \quad (19)$$

2.3 Phy-X/PSD program and XCOM

Photon Shielding and Dosimetry (PSD) well known as Phy-X/PSD is a user-friendly for simulation of shielding parameters available at <https://phy-x.net/PSD> [19] and XCOM online program [20]. Saleh et al. [21] utilized XCOM software to calculate the nuclear radiation shielding properties of lithium lead bismuth borate glass and compare with Phy-X/PSD program. The shielding parameters show a good agreement with less than 1% deviation. For this study, we employ Phy-X/PSD to investigate the shielding parameters of the bismuth borate glass doped MnO₂.

The linear attenuation coefficient LAC is a parameter that describes the fraction of monoenergetic photons that are absorbed per unit thickness of a material and is given by [22].

$$I = I_o e^{-\mu t} \quad (20)$$

where I represent the fraction of photons after interaction with an absorber, I_o represent the incident photon intensity before interaction with an absorber material, μ is a constant called the linear attenuation coefficient (cm⁻¹) of the absorbing material and t is the material thickness (cm).

Mass attenuation coefficient is a quantity that described the ability of gamma photons to penetrate a material medium per unit mass [23].

$$\mu_m = \mu / \rho = \sum_i w_i (\mu / \rho)_i \quad (21)$$

where w_i is weight fraction of the i th compound and ρ is the density (g/cm³) of the absorber material.

Half value layer describes how much thickness (cm) of a material absorber that is just sufficient to attenuate/absorbed the incident photon intensity by ½ of its original intensity [24].

$$HVL = \ln 2 / \mu \quad (22)$$

Tenth value layer describes how much thickness of an absorber material that is sufficient enough to reduce the incident photon intensity by 1/10 of its original intensity [25].

$$TVL = \ln 10 / \mu \quad (23)$$

Mean free path is a parameter that described the mean distance travelled by photons in an absorber material before a successful interaction [22].

$$MFP = 1/\mu \quad (24)$$

Effective atomic number and effective electron density are quantities that quantify the ability of a material to interact and absorbed photon radiation. It depends on the atomic number of the composition and effective electronic state of the absorber. The following equations can be used to calculate Z_{eff} and N_{eff} [19].

$$Z_{eff} = \sigma_T/\sigma_e \quad (25)$$

Total atomic cross section

$$\sigma_T = \mu_m M / N_A \quad (26)$$

where M represent the atomic mass of absorber material and N_A , is the Avogadro's constant.

Electronic cross section

$$\sigma_e = \sigma_T / Z_{eff} \quad (27)$$

Effective electron density is given by

$$N_{eff} = \mu_m / \sigma_e = (\sum_i f_i A_i / \sum_i f_i A_i) Z_{eff} \sum n_i \quad (28)$$

where $\sum n_i$ is the summation of the number of ith elements making up the absorber material.

The percentage deviation for the two different software's can be written as:

$$Dev. (\%) = \frac{\left(\frac{\mu}{\rho}\right)_{PHY-X} - \left(\frac{\mu}{\rho}\right)_{XCOM}}{\left(\frac{\mu}{\rho}\right)_{PHY-X}} \times 100 \quad (29)$$

3. Results and Discussion

The optical properties including refractive index n , dielectric constant ϵ , ions concentrations N , interatomic spacing, electric susceptibility χ , transmission coefficient, reflection loss R_i , metallization $M(n)$, electron polarizability α^e , optical electronegativity η_j , and optical basicity λ are tabulated in Table 2.

The refractive index of the MnBiSi glass decreased from 2.71 to 1.68 with increasing ions concentration from 1.35 to 1.62 cm^{-3} as a result of decreased in the glass density from 6.796 to 6.142 g/cm^3 . This can be attributed to an increased in formation of non-bridging oxygen. Furthermore, Manganese ions have lower polarization compared to 0MnBiSi glass, as such, increasing MnO_2 level decreased the electronic polarizability and refractive index as shown in

Fig. 1. The interatomic spacing in the glass structure reduced as the concentration of ions in MnO_2 increased, resulting in tighter bonds and thus improved glass stiffness as seen in Fig. 2.

The glass sample's ability to transmit light within the visible region is 88% for 20MnBiSi and 65% for 0MnBiSi glass, demonstrating the influence of dopant content expanding the network, which results in lowering absorption center and hence, increased light transmission and a reduction in reflection loss as seen in Fig. 3. The $M(n)$ as shown in Table 2 satisfy the non-metallic condition ($0 < R_m/V_m < 1$).

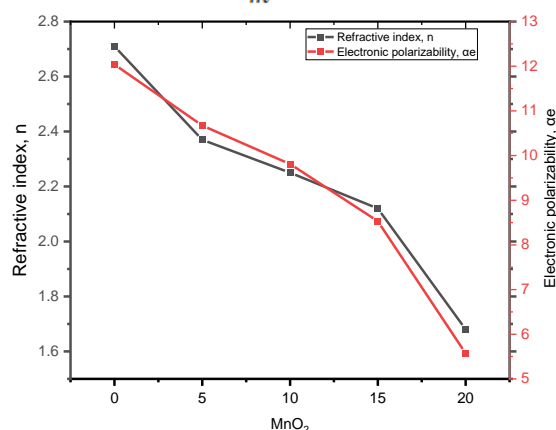


Fig. 1 The effect of MnO_2 on the refractive index, electronic polarizability in MnBiSi glass.

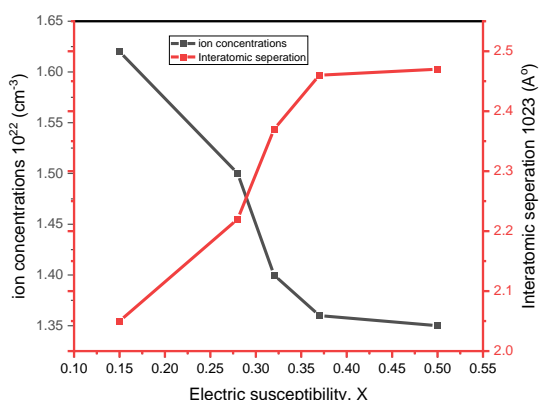


Fig. 2. Relationship between ions concentrations, interatomic separation, and electric susceptibility.

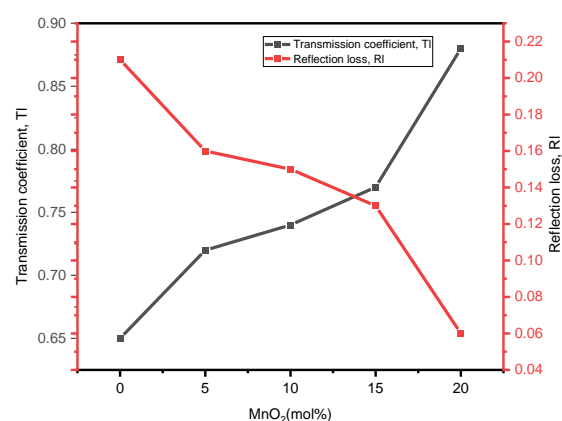


Fig. 3. Shows how MnBiSi glasses responds to light transmission, reflection, and MnO_2 concentrations.

3.1 Elastic and mechanical properties

The elastic properties of glass, particularly the elastic modulus, play a crucial role in radiation shielding effectiveness. A higher elastic modulus indicates a glass's ability to resist mechanical deformation. The addition of MnO₂ to bismuth silicate glass increases its elastic modulus (see Table 3), resulting in a stiffer material with improved resistance to deformation and corrosion. This enhancement in elastic properties contributes to improved radiation shielding performance [26]. The glass sample

20MnBiSi has the highest elastic moduli and atomic packing density, resulting in stronger interatomic bonds and smaller distances between atoms. This makes it the most resistant to elastic deformation. In contrast, sample 0MnBiSi has the lowest elastic moduli and largest atomic distances, making it the most susceptible to elastic deformation.

Table 2. Optical characteristics of MnBiSi glasses

Parameters	0MnBiSi	5MnBiSi	10MnBiSi	15MnBiSi	20MnBiSi
Molecular weight, M_w	303.61	284.66	265.71	246.75	227.80
Refractive index, n	2.71	2.37	2.25	2.12	1.68
dielectric constant ϵ	7.34	5.60	5.08	4.48	2.83
molar refractivity, R_m	30.34	26.88	24.72	21.51	14.05
Ion's concentration, $N * 10^{22}$ cm ⁻³	1.35	1.36	1.40	1.50	1.62
Interatomic separation, $*10^{23}$ (Å ⁰)	2.47	2.46	2.37	2.22	2.05
Electronic polarizability, α_e	12.04	10.67	9.81	8.53	5.57
Transmission coefficient, T_c	0.65	0.72	0.74	0.77	0.88
Reflection loss, R_r	0.21	0.16	0.15	0.13	0.06
Metallization M(n)	0.31	0.44	0.49	0.56	0.83
Optical electronegativity η	0.74	0.59	0.55	0.49	0.34
electron polarizability α	2.83	2.97	3.01	3.06	3.19
optical basicity Λ	1.33	1.40	1.43	1.45	1.53
Number of oxygen atom	2.60	2.55	2.50	2.45	2.40
polaron interaction r_p	0.065	0.064	0.062	0.058	0.054
Electric susceptibility, χ	0.50	0.37	0.32	0.28	0.15

Table 3. Summary of elastic and mechanical properties of MnBiSi glasses.

Glass sample code	V_T (cm ³ /mol)	G_I KJ/mol	E_T Gpa	K_T Gpa	S_T Gpa	L_T Gpa	P_r	H_m	F_r
0MnBiSi	0.73	48.93	298.61	260.75	404.51	800.10	0.304	14.93	6.21
5MnBiSi	0.71	50.55	300.04	254.82	408.24	799.14	0.299	15.49	6.41
10MnBiSi	0.72	51.55	310.29	267.24	421.24	828.89	0.302	15.77	6.31
15MnBiSi	0.73	52.55	320.70	280.04	434.44	859.29	0.304	16.04	6.21
20MnBiSi	0.74	53.55	331.28	293.24	447.83	890.35	0.307	16.31	6.11

Table 4. Comparison of mass attenuation coefficient of some fabricated glass with excellent shielding properties

Glass code	Photon energy (MeV)				Ref.
	0.015	0.1	0.6	3	
BPNC6	70.582	3.495	0.107	0.04	[27]
TAW-D	47.69	1.674	0.083	0.037	[28]
BBNS6	63.216	3.011	0.102	0.039	[29]
TZN-A	42.56	1.394	0.08	0.036	[30]
0MnBiSi	96.415	4.767	0.12	0.042	This work
5 MnBiSi	94.801	4.666	0.119	0.042	This work
10MnBiSi	92.956	4.551	0.118	0.41	This work
15MnBiSi	90.828	4.417	0.116	0041	This work
20MnBiSi	88.346	4.262	0.115	0.041	This work

Table 5. Mass attenuation coefficient of the investigated 15MnBiSi, 20MnBiSi glasses via Phy-X/PSD

Energy (MeV)	15MnBiSi			20MnBiSi		
	Phy-X	XCOM	Dev.%	Phy-X	XCOM	Dev.%
0.015	90.828	90.86	0.04	88.346	88.32	0.03
0.02	69.321	69.34	0.03	67.145	67.13	0.02
0.03	24.386	24.39	0.02	23.608	23.6	0.03
0.04	11.576	11.58	0.03	11.204	11.2	0.03
0.05	6.497	6.499	0.03	6.289	6.287	0.03
0.06	4.069	4.07	0.02	3.939	3.939	0.0
0.08	1.977	1.977	0	1.916	1.915	0.05
0.1	4.417	4.419	0.05	4.262	4.261	0.02
0.15	1.622	1.622	0	1.567	1.567	0.0
0.2	0.818	0.817	0.12	0.792	0.792	0.0
0.3	0.343	0.342	0.3	0.334	0.334	0.0
0.4	0.205	0.204	0.5	0.201	0.2	0.5
0.5	0.147	0.146	0.7	0.144	0.144	0.0
0.6	0.116	0.116	0	0.115	0.114	0.87
0.8	0.086	0.085	1.2	0.085	0.084	1.18
1	0.07	0.069	1.43	0.07	0.069	1.43
1.5	0.052	0.053	1.92	0.052	0.052	0.0
2	0.046	0.046	0	0.046	0.045	2.17
3	0.041	0.042	2.38	0.041	0.04	2.4
4	0.04	0.041	2.5	0.04	0.039	2.5
5	0.04	0.04	0	0.039	0.039	0.0
6	0.04	0.039	2.5	0.04	0.039	2.5
7	0.041	0.04	2.4	0.04	0.04	0.0
8	0.042	0.041	2.38	0.041	0.041	0.0
9	0.043	0.042	2.32	0.042	0.042	0.0
10	0.044	0.043	2.27	0.043	0.043	0.0
11	0.045	0.044	2.22	0.044	0.043	2.27
12	0.046	0.045	2.17	0.045	0.044	2.22
13	0.047	0.046	2.12	0.046	0.045	2.17
14	0.048	0.047	2.08	0.047	0.046	2.13
15	0.049	0.048	2.04	0.048	0.047	2.08

The Poisson's ratio decreases from 0MnBiSi to 5MnBiSi, but then increases significantly from 5MnBiSi to 20MnBiSi, indicating a reduction in defects and improvement in the glass structure. The fractional bond connectivity increases from 0MnBiSi to 5MnBiSi, indicating increased connectivity and rigidity, but then decreases slightly from 5MnBiSi to 20MnBiSi. The 5MnBiSi glass has the highest connectivity value of 6.41, suggesting optimal structural properties. The decreasing effect in F_r can be attributed to the amount of bridging oxygen decreasing while increasing the non-bridging oxygen resulting in decreasing glass density (see Table 1).

The microhardness of the glasses increased as the mol% of MnO₂ increased, with the highest microhardness (16.31) found in the 20MnBiSi glass and the lowest (14.93) in the 0MnBiSi glass as shown in Table 3. This suggests that the

20MnBiSi glass has the greatest elastic and mechanical advantages compared to the other samples.

3.2 Radiation shielding properties

To study MnBiSi glasses as potential photon radiation blockers, mass attenuation coefficients were estimated using the Phy-X/PSD program and compared to XCOM in the photon energy range of 0.015-15 MeV. Table 5 displays the mass attenuation coefficients of the MnBiSi glasses examined using Phy-X/PSD and XCOM, as well as their percentage deviation. The deviation of the MnBiSi glass MAC values from the Phy-X and XCOM results is less than 3% for all photon energy range, demonstrating the accuracy of MAC results. Fig. 4 displays MAC behavior as a function of photon energy and MnBiSi glass density.

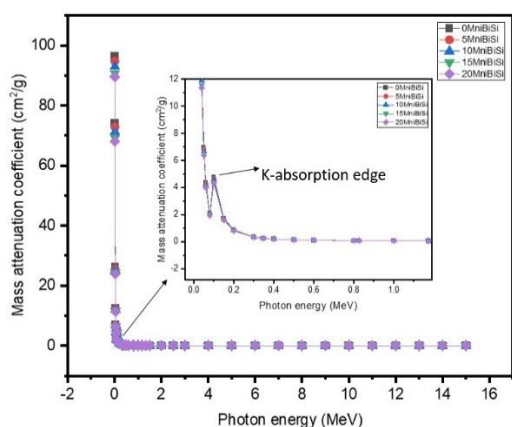


Fig. 4. MAC as a function of photon energy of the MnBiSi glasses

The MAC of MnBiSi sample glasses with varying MnO₂ levels is shown in Fig. 4. The mass attenuation coefficient of MnBiSi exhibits greater MAC values at lower photon energies due to increased photon absorption mediated by the photoelectric effect. The MAC (mass attenuation coefficient) values at 0.015 MeV decrease as the mol% of MnO₂ increases from 0MnBiSi to 20MnBiSi. The highest MAC value (96.415 cm²/g) is observed in 0MnBiSi, attributed to its higher density. The addition of MnO₂ reduces the MAC due to the replacement of higher molecular mass Bi₂O₃ with lower molecular mass MnO₂, resulting in fewer electrons available to interact with incident photons and decreased photon absorption due to density differences. The sharp drop in photon absorption within the photon energy range of 0.015–0.15 MeV is dominated by photoelectric effect and the attenuation coefficient is proportional to the Z^{4-5} and inversely to E^3 in this region as suggested by others [31], [32], [33]. The dramatic decline in attenuation around 90.5 KeV is due to overcoming bismuth's binding energy, which allows X-rays to be captured by the k-shell electrons. The mass attenuation coefficient gradually decreased as photon energy increased from 0.2 MeV to 3 MeV, and can be attributed to multiple scattering caused by deeper photon penetration, resulting in an increased scattering and reduction in photon absorption where Z varies E^{-1} holds. This region is called the Compton scattering region. Above the region of Compton scattering, a pairing phenomenon occurs at 4 MeV and above, the MAC values behave like semi-constant and varies with $\log E$ and Z^2 where pair production event dominates the interaction process. The addition of MnO₂ to bismuth silicate glasses, at the expense of bismuth, decreases their radiation shielding effectiveness. The mass attenuation coefficient (MAC) of these glasses was compared to other

fabricated glasses at specific photon energies, as shown in Table 5.

The shielding effectiveness of the investigated glass can also be assessed using HVL. The glass sample with the lowest HVL is desirable, as smaller HVL requires a smaller thickness to absorb photon radiation [34]. The thickness (cm) required to reduce the incident photon intensity by a factor $\frac{1}{2}$ is term as half value layer. According to Fig. 5, the 0MnBiSi glass sample has the lowest HVL (0.15 cm) compared to 5MnBiSi (0.16 cm), 10MnBiSi (0.17), 15MnBiSi (0.17), and 20MnBiSi (0.18 cm), respectively. As shown in Fig. 5, 0MnBiSi has the highest photon attenuation properties due to its larger electron density per unit volume, which aids scattering and photon absorption.

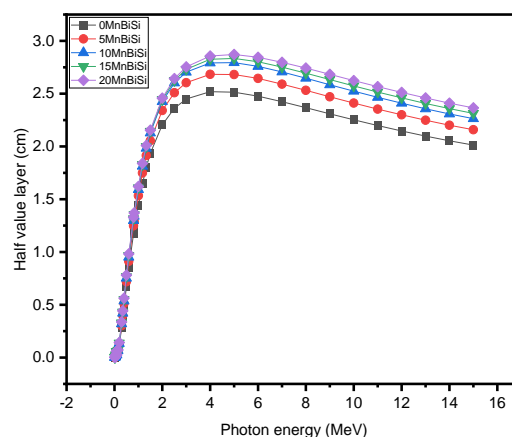


Fig 5. Half value layer as function of photon energy of the MnBiSi glass samples.

This means that a 0.049 cm thick HVL of the 0MnBiSi sample will lower gamma photon intensity to one-half of its original intensity, as will 5MnBiSi, 10MnBiSi, 15MnBiSi, and 20MnBiSi samples with thicknesses of 0.053, 0.056, 0.058, and 0.060 cm, respectively.

In the photoelectric region at low photon energies, the mean free path (MFP) values increase and are highest for the 0MnBiSi glass sample, which has the highest effective atomic number. The 0MnBiSi glass sample has the highest photon absorption in the photoelectric region. As photon energy increases, the mean free path (MFP) increases rapidly, indicating a shift to Compton scattering dominance. Generally, MFP increases with photon energy as seen in Fig. 6. However, 0MnBiSi sample has the lowest MFP value compared to the other samples in the series. Glasses as MnO₂ to Bi₂O₃ substitution increases throughout the glass system, the glass density decreases and the MFP decreases.

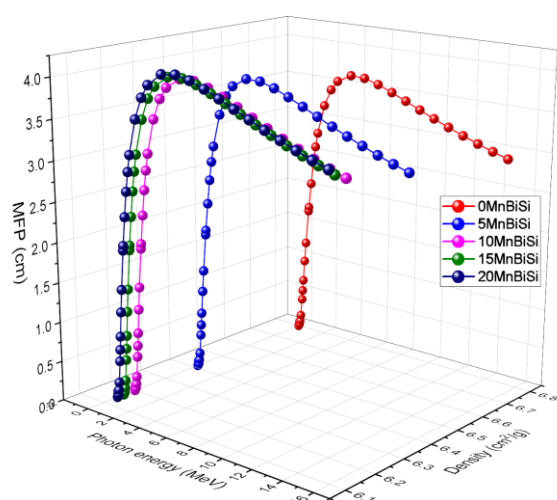


Fig. 6. Variation of MFP as function of MnBiSi glass density and photon energy

4. Conclusion

The Optical, elastic, mechanical, and radiation shielding efficacy of manganese bismuth silicate glass with composition $(60-x)\text{Bi}_2\text{O}_3+\text{SiO}_2+x\text{MnO}_2$, where $x=0,5,10,15$, and 20 , is examined. When 20 mol% of MnO_2 is doped into the glass, the optical clarity (refractive index) increases by approximately 61.3% compared to undoped glass and 35.4% increase in transmission of light in the visible region. The 20MnBiSi sample, with the highest elastic moduli, has the highest resistance to elastic deformation due to its highest atomic packing density. Additionally, its microhardness is 9.25% higher than that of the 0MnBiSi sample, indicating superior mechanical properties. The radiation attenuation properties of the glasses were simulated using Phy-X/PSD and XCOM software, showing that sample 0MnBiSi of density 6.796 g/cm^3 has the highest radiation absorption capabilities. While sample 20MnBiSi excels in optical, elastic, and mechanical properties, making it suitable for applications optical clarity, strength, and durability is paramount. Sample 0MnBiSi remains the best choice when high radiation absorption is the primary requirement due to its superior attenuation coefficients and lower half-value layer (HVL) and mean free path (MFP) as compared to other investigated samples.

Conflict of interest

The authors declare no conflict of interest.

Acknowledgements

The authors express their gratitude to the Tertiary Education Trust Fund (TETFund) Nigeria (ETF/ES/UNIV/SOKOTO/TSAS/2020) and Sokoto State University for their support of my PhD studies. Additionally, they acknowledge the

Department of Physics, University Technology Malaysia, for providing a conducive environment and necessary resources that facilitated the successful completion of this research.

References

- Abuelhia, E. and A. Alghamdi, *Evaluation of arising exposure of ionizing radiation from computed tomography and the associated health concerns*. Journal of radiation research and applied sciences, 2020. **13**(1): p. 295-300. <https://doi.org/10.1080/16878507.2020.1728962>
- Kaur, P., D. Singh, and T. Singh, *Heavy metal oxide glasses as gamma rays shielding material*. Nuclear Engineering and design, 2016. **307**: p. 364-376. <https://doi.org/10.1016/j.nucengdes.2016.07.029>
- Singh, V.P., N. Badiger, and J. Kaewkhao, *Radiation shielding competence of silicate and borate heavy metal oxide glasses: comparative study*. J. Non-Cryst. Solids, 2014. **404**: p. 167-173. <https://doi.org/10.1016/j.jnoncrystal.2014.08.003>
- Tekin, H., O. Kilicoglu, E. Kavaz, E. Altunsoy, M. Almatari, O. Agar, and M. Sayyed, *The investigation of gamma-ray and neutron shielding parameters of Na2O-CaO-P2O5-SiO2 bioactive glasses using MCNPX code*. Results Phys., 2019. **12**: p. 1797-1804. <https://doi.org/10.1016/j.rinp.2019.02.017>
- Madheshiya, A., C. Gautam, and K.K. Srivastava, *Fabrication of lead-bismuth titanate borosilicate glass ceramics and dielectric characteristics doped with GNPs*. Materials Research Express, 2020. **7**(1): p. 015206. DOI 10.1088/2053-1591/ab67ff
- Halimah, M., A. Azuraida, M. Ishak, and L. Hasnimulyati, *Influence of bismuth oxide on gamma radiation shielding properties of borotellurite glass*. J. Non-Cryst. Solids, 2019. **512**: p. 140-147. <https://doi.org/10.1016/j.jnoncrystal.2019.03.004>
- Sallam, O., A. Madbouly, N. Elalaily, and F. Ezz-Eldin, *Physical properties and radiation shielding parameters of bismuth borate glasses doped transition metals*. J. Alloys Compd., 2020. **843**: p. 156056. <https://doi.org/10.1016/j.jallcom.2020.156056>
- ElBatal, F., M. Marzouk, and A. Abdel Ghany, *Gamma rays interaction with bismuth borate glasses doped by transition metal ions*. Journal of materials science, 2011. **46**: p. 5140-5152. DOI 10.1007/s10853-011-5445-4
- Terczyńska-Madej, A., K. Cholewa-Kowalska, and M. Łączka, *Coordination and valence state of transition metal ions in alkali-borate*

- glasses. *Opt. Mater.*, 2011. **33**(12): p. 1984-1988.
<https://doi.org/10.1016/j.optmat.2011.03.046>
10. Dult, M., R. Kundu, N. Berwal, R. Punia, and N. Kishore, *Manganese modified structural and optical properties of bismuth silicate glasses*. *J. Mol. Struct.*, 2015. **1089**: p. 32-37.
<https://doi.org/10.1016/j.molstruc.2015.02.025>
 11. Eevon, C., M. Halimah, A. Zakaria, C. Azurahaman, M. Azlan, and M. Faznny, *Linear and nonlinear optical properties of Gd³⁺ doped zinc borotellurite glasses for all-optical switching applications*. *Results Phys.*, 2016. **6**: p. 761-766.
<https://doi.org/10.1016/j.rinp.2016.10.010>
 12. Linda, D., J.-R. Duclère, T. Hayakawa, M. Dutreilh-Colas, T. Cardinal, A. Mirgorodsky, A. Kabadou, and P. Thomas, *Optical properties of tellurite glasses elaborated within the TeO₂-Ti₂O-Ag₂O and TeO₂-ZnO-Ag₂O ternary systems*. *J. Alloys Compd.*, 2013. **561**: p. 151-160.
<https://doi.org/10.1016/j.jallcom.2013.01.172>
 13. Umar, S., M. Halimah, K. Chan, and A. Latif, *Polarizability, optical basicity and electric susceptibility of Er³⁺ doped silicate borotellurite glasses*. *J. Non-Cryst. Solids*, 2017. **471**: p. 101-109.
<https://doi.org/10.1016/j.jnoncrysol.2017.05.018>
 14. Thakur, S., V. Thakur, A. Kaur, and L. Singh, *Structural, optical and thermal properties of nickel doped bismuth borate glasses*. *J. Non-Cryst. Solids*, 2019. **512**: p. 60-71.
<https://doi.org/10.1016/j.jnoncrysol.2019.02.012>
 15. Dimitrov, V. and S. Sakka, *Linear and nonlinear optical properties of simple oxides. II*. *J. Appl. Phys.*, 1996. **79**(3): p. 1741-1745.
<https://doi.org/10.1063/1.360963>
 16. Khattari, Z., N.A. Alsaif, Y. Rammah, E. Abou Hussein, M. Shams, and R. Elsad, *Fabrication, physical, mechanical, and radiation protection properties of bismoborate glasses containing La³⁺ Eu³⁺ as additive ions*. *Radiat. Phys. Chem.*, 2022. **201**: p. 110454.
<https://doi.org/10.1016/j.radphyschem.2022.110454>
 17. Inaba, S., S. Fujino, and K. Morinaga, *Young's modulus and compositional parameters of oxide glasses*. *J. Am. Ceram. Soc.*, 1999. **82**(12): p. 3501-3507.
<https://doi.org/10.1111/j.1151-2916.1999.tb02272.x>
 18. Al-Buriahi, M., T. Taha, M.A. Alothman, H. Donya, and I. Olarinoe, *Influence of WO₃ incorporation on synthesis, optical, elastic and radiation shielding properties of borosilicate glass system*. *Eur. Phys. J. Plus*. 2021. **136**(7): p. 779.
<https://doi.org/10.1140/epjp/s13360-021-01790-5>
 19. Şakar, E., Ö.F. Özpolat, B. Alım, M. Sayyed, and M. Kurudirek, *Phys-X/PSD: development of a user friendly online software for calculation of parameters relevant to radiation shielding and dosimetry*. *Radiat. Phys. Chem.*, 2020. **166**: p. 108496.
<https://doi.org/10.1016/j.radphyschem.2019.108496>
 20. Berger, M.J., *XCOM: photon cross sections database*. <http://physics.nist.gov/PhysRefData/Xcom/Text/XCOM.html>, 1998. **8**: p. 3587.
<http://www.nist.gov/pml/data/xcom/index.cfm> 2010.
 21. Saleh, E.E., M.A. Algradee, S. El-Fiki, and G. Youssef, *Fabrication of novel lithium lead bismuth borate glasses for nuclear radiation shielding*. *Radiat. Phys. Chem.*, 2022. **193**: p. 109939.
<https://doi.org/10.1016/j.radphyschem.2021.109939>
 22. Kumar, A., D. Gaikwad, S.S. Obaid, H. Tekin, O. Agar, and M. Sayyed, *Experimental studies and Monte Carlo simulations on gamma ray shielding competence of (30+ x) PbO10WO₃ 10Na₂O- 10MgO-(40-x) B₂O₃ glasses*. *Prog. Nucl. Energy*, 2020. **119**: p. 103047.
<https://doi.org/10.1016/j.pnucene.2019.103047>
 23. Tekin, H., E. Kavaz, A. Papachristodoulou, M. Kamislioglu, O. Agar, E.A. Guclu, O. Kilicoglu, and M. Sayyed, *Characterization of SiO₂-PbO-CdO-Ga₂O₃ glasses for comprehensive nuclear shielding performance: Alpha, proton, gamma, neutron radiation*. *Ceram. Int.*, 2019. **45**(15): p. 19206-19222.
<https://doi.org/10.1016/j.ceramint.2019.06.168>
 24. Agar, O., M. Sayyed, F. Akman, H. Tekin, and M. Kaçal, *An extensive investigation on gamma ray shielding features of Pd/Ag-based alloys*. *Nucl. Eng. Technol.*, 2019. **51**(3): p. 853-859.
<https://doi.org/10.1016/j.net.2018.12.014>
 25. Sayyed, M., A. Kumar, H. Tekin, R. Kaur, M. Singh, O. Agar, and M.U. Khandaker, *Evaluation of gamma-ray and neutron shielding features of heavy metals doped Bi₂O₃-BaO-Na₂O-MgO-B₂O₃ glass systems*. *Prog. Nucl. Energy*, 2020. **118**: p. 103118.
<https://doi.org/10.1016/j.pnucene.2019.103118>
 26. Li, H. and Y. Zheng, *Recent advances in bulk metallic glasses for biomedical applications*. *Acta biomaterialia*, 2016. **36**: p. 1-20.
<https://doi.org/10.1016/j.actbio.2016.03.047>
 27. Al-Buriahi, M., Y. Alajerami, A. Abouhaswa, A. Alalawi, T. Nutaro, and B. Tonguc, *Effect of*

- chromium oxide on the physical, optical, and radiation shielding properties of lead sodium borate glasses. *J. Non-Cryst. Solids*, 2020. **544**: p. 120171. <https://doi.org/10.1016/j.jnoncrysol.2020.120171>
28. Al-Buriah, M., V. Singh, A. Alalawi, C. Sriwunkum, and B.T. Tonguc, *Mechanical features and radiation shielding properties of TeO₂-Ag₂O-WO₃ glasses*. *Ceram. Int.*, 2020. **46**(10): p. 15464-15472. <https://doi.org/10.1016/j.ceramint.2020.03.091>
29. Abouhaswa, A., M. Mhareb, A. Alalawi, and M. Al-Buriah, *Physical, structural, optical, and radiation shielding properties of B₂O₃-20Bi₂O₃-20Na₂O₂-Sb₂O₃ glasses: Role of Sb₂O₃*. *J. Non-Cryst. Solids*, 2020. **543**: p. 120130. <https://doi.org/10.1016/j.jnoncrysol.2020.120130>
30. Al-Buriah, M., E.M. Bakhsh, B. Tonguc, and S.B. Khan, *Mechanical and radiation shielding properties of tellurite glasses doped with ZnO and NiO*. *Ceram. Int.*, 2020. **46**(11): p. 19078-19083. <https://doi.org/10.1016/j.ceramint.2020.04.240>
31. Tonguc, B.T., H. Arslan, and M.S. Al-Buriah, *Studies on mass attenuation coefficients, effective atomic numbers and electron densities for some biomolecules*. *Radiat. Phys. Chem.*, 2018. **153**: p. 86-91. <https://doi.org/10.1016/j.radphyschem.2018.08.025>
32. Alduhaibat, M.J., M.S. Amana, N.J. Jubier, and A. Salim, *Improved gamma radiation shielding traits of epoxy composites: Evaluation of mass attenuation coefficient, effective atomic and electron number*. *Radiat. Phys. Chem.*, 2021. **179**: p. 109183. <https://doi.org/10.1016/j.radphyschem.2020.109183>
33. Al-Hadeethi, Y., M. Al-Buriah, and M. Sayyed, *Bioactive glasses and the impact of Si₃N₄ doping on the photon attenuation up to radiotherapy energies*. *Ceram. Int.*, 2020. **46**(4): p. 5306-5314. <https://doi.org/10.1016/j.ceramint.2019.10.281>
34. Obaid, S.S., M. Sayyed, D. Gaikwad, and P.P. Pawar, *Attenuation coefficients and exposure buildup factor of some rocks for gamma ray shielding applications*. *Radiat. Phys. Chem.*, 2018. **148**: p. 86-94. <https://doi.org/10.1016/j.radphyschem.2018.02.026>